Multifragment production in heavy ion induced reactions at intermediate energy

R. Dayras, G. Auger, C O. Bacri, A. Benkirane, J. Benlliure, B. Berthier, E. Bisquer, B. Borderie, P. Box, R. Brou, et al.

BB

CEA/SACLAY
DSM

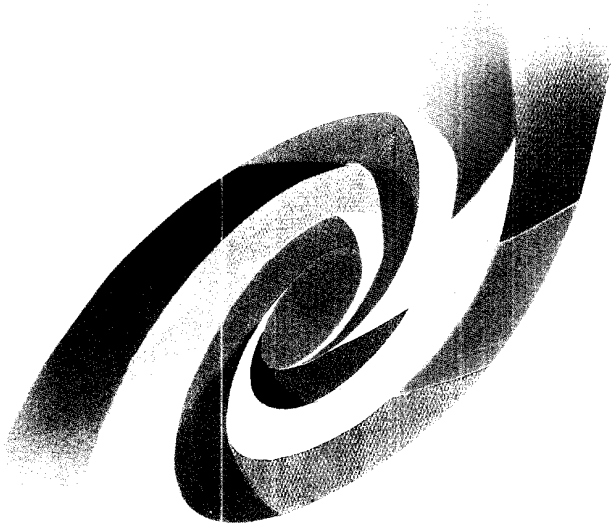

SW9833

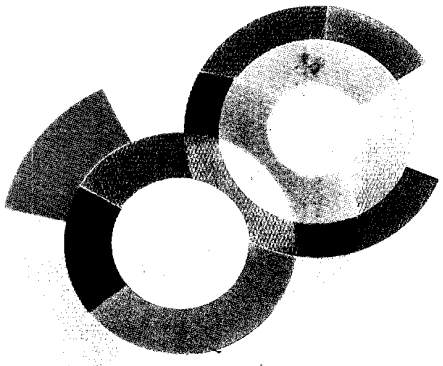

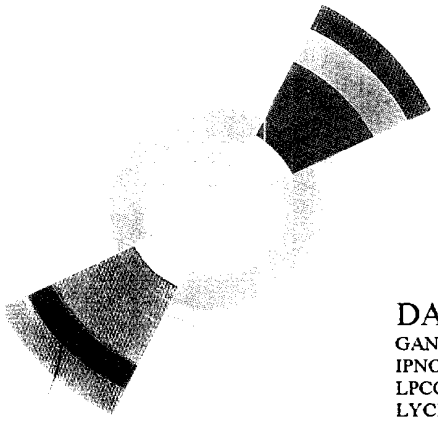

DAPNIA/SPhN-97-14 03/1997
GANIL P97-06
IPNO-DRE-97-06
LPCC 97-02
LYCEN/9705
SUBATECH 97-05

Multifragment production in heavy ion induced reactions at intermediate energy

DAPNIA

R. Dayras
for the INDRA Collaboration

Département d'**A**strophysique, de Physique des **P**articules, de Physique **N**ucléaire et de l'**I**nstrumentation **A**ssociée
CEA/Saclay F-91191 Gif-sur-Yvette Cédex

Couverture Sylvie Cabrit et Marc Sauvage

237444

Contribution au 7ème Colloque Franco-Japonais:
«Frontier and Perspectives of Nuclear Science»
DOGASHIMA (Japon), 30-09/04-10/1996

Multifragment production in heavy ion induced reactions at intermediate energy

R. Dayras[1)]

for the **INDRA Collaboration**

G. Auger[2)], Ch.O. Bacri[3)], A. Benkirane[2)], J.Benlliure[2)], B. Berthier[1-a)], E. Bisquer[6)], B. Borderie[3)], R. Bougault[4)], P. Box[3)], R. Brou[4)], Ph. Buchet[1)], Y. Cassagnou[1)], J.L. Charvet[1)], A. Chbihi[2)], J. Colin[5)], D. Cussol[4)], E. De Filippo[1-b)], A. Demeyer[6)], D. Doré[3)], D. Durand[4)], P. Ecomard[2)], P. Eudes[5)], A. Genoux-Lubain[4-c)], E. Gerlic[6)], D. Gourio[5)], D. Guinet[6)], F. Gulminelli[4)], R. Laforest[4)], L. Lakehal-Ayat[3)], P. Lautesse[6)], J.L. Laville[5)], L. Lebreton[6)], C. Lebrun[4)], J.F. Lecolley[4)], A. Le Fèvre[2)], T. Lefort[4)], R. Legrain[1)], O. Lopez[4)], M. Louvel[4)], J. Lukasik[3-d)], M. Mahi[4)], N. Marie[2)], V. Métivier[4-e)], T. Nakagawa[4-f)], L. Nalpas[1)], A. Ouatizerga[3)], M. Parlog[3-g)], E. Plagnol[3)], J. Péter[4)], E.C. Pollacco[1)], A. Rahmani[5)], R. Regimbart[4)], T. Reposeur[5)], M.F. Rivet[3)], E. Rosato[4-h)], F. Saint-Laurent[2-i)], A. Siwek[4)], M. Squalli[3)], J.C. Steckmeyer[4)], M. Stern[6)], B. Tamain[4)], L. Tassan-Got[3)], E. Vient[4)], C. Volant[1)], J.P. Wieleczko[2-j)], A. Wieloch[4)], Ma Y.-G.[4)], K. Yuasa-Nakagawa[4-f)]

1) CEA, DAPNIA/SPhN, CE Saclay, 91191 Gif sur Yvette Cedex, France
2) GANIL, CEA et IN2P3-CNRS, B.P. 5027, 14021 Caen Cedex, France
3) IPN, IN2P3-CNRS, 91406 Orsay Cedex, France
4) LPC, IN2P3-CNRS et Université, 14050 Caen Cedex, France
5) SUBATECH, IN2P3-CNRS et Université, 44072 Nantes Cedex 03, France
6) IPN Lyon, IN2P3-CNRS et Université, 69622 Villeurbanne, Cedex, France

Abstract

Using the 4π multidetector array INDRA at GANIL, we have investigated the reaction $^{36}Ar+^{58}Ni$ for bombarding energies ranging from 32 to 95 AMeV. Over this energy domain, quasi-binary dissipative collisions are the dominant process exhausting more than 90% of the reaction cross-section. The excitation energy is shared almost equally between the quasi-projectile and the quasi-target, suggesting that the interaction time is too short to permit thermalization of the whole system. However, the kinematical properties and the chemical composition of the disintegration products of the quasi-projectile and of the quasi-target (which decay independently) are consistent with local thermodynamical equilibrium. At the highest bombarding energy, excitation energies in excess of 25 AMeV are reached. For excitation energies greater than 6 AMeV, vaporization (events in which only light particles, $Z \leq 2$, are produced) sets in. A survey of the nuclear caloric curve, the evolution of the temperature as a function of the excitation energy, in the quasi-projectile does not show evidence of a plateau as a possible signature of a liquid-gas phase transition.

Present addresses

a) CEA, DRECAM, Laboratoire Pierre Sue, CE Saclay, 91191, Gif-sur-Yvette Cedex, France
b) Istituto Naz. Fisica Nucleare and Dipatimento di Fisica, Corso Italia 57, 95129 Catania, Italy
c) Institut Universitaire de Technologie, BP 408, 03107 Montluçon Cedex, France
d) Institute of Nuclear Physics, ul, Radzikowskiego 152, 31-342 Kraków, Poland
e) SUBATECH, IN2P3-CNRS et Université, 44072 Nantes Cedex 03, France
f) Cyclotron Laboratory, RIKEN, 2-1 Hirosawa, Wako, Saitama,351-01, Japan
g) Institute of Physics and Nuclear Engineering, IFA, P.O. Box MG6, Bucharest, Romania
h) Dipartimento di Science Fisiche, Univ. di Napoli, 80125 Napoli, Italy
i) CEA, DRFC/STEP, CE Cadarache, 1308 Saint Paul lez Durance Cedex, France
j) Institute of Physics, Jagellonian University, Reymonta 4, 30059, Kraków, Poland

1. Introduction

The determination of the properties of highly excited nuclei created in nucleus-nucleus collisions has become one of the major axis of research in nuclear physics in recent years and is the subject of numerous theoretical as well as experimental investigations. At stake are the limit of stability of the nucleus[1,2], the appearance of new decay modes[3,4], the nuclear matter phase diagram[5] and ultimately the nuclear equation of state[5].

Experimentally, the basic difficulties reside in disentangling the intrinsic properties of the hot nuclei formed in nucleus-nucleus collisions from dynamically induced effects. Whereas the reaction mechanisms are relatively well understood at low incident energies (<20 MeV/nucleon) where mean field effects dominate and at high incident energies (>200 MeV/nucleon) where nucleon-nucleon collisions are the dominant process, this is not the case in the intermediate energy range where both the mean field and nucleon-nucleon collisions enter into play.

The recent advent of 4π detection arrays with high geometrical efficiency, good granularity and low detection energy thresholds has enabled us to elucidate several aspects concerning the main reaction mechanisms. It is now well established that the intermediate energy regime (20 MeV<E_{inc}/A<100 MeV) is characterized by a dominance of quasi-binary dissipative interactions in which a quasi-projectile and a quasi-target emerge from the collisions with an excitation energy which increases as the impact parameter decreases. However, in contrast with deep inelastic collisions at low energy (~10 MeV/nucleon), the zone of overlap between projectile and target is subjected to a strong emission of particles and fragments (mid-rapidity emission) thus introducing a departure from a purely binary process. Only the most central collisions lead to an (in)complete fusion process which disappears altogether above ~50 MeV/nucleon for intermediate mass systems as the one under consideration here. The essentially binary nature of the collisions permits to produce well characterized projectile-like and target-like nuclei over a broad range of excitation energies which may reach and even exceed the available center of mass energy. This offers the unique opportunity to explore the decay modes of these nuclei with excitation energy, from standard evaporation to full vaporization in passing through the multifragmentation regime.

2. Experimental method.

The 4π detection array INDRA at GANIL was used to investigate the reaction $^{36}Ar+^{58}Ni$ at 32, 40, 52, 63, 74, 84 and 95 MeV/nucleon. INDRA, a detailed description of which can be found elsewhere[6-8], can be considered as an ensemble of 336 telescopes covering 90% of the 4π solid angle. The detection cells are distributed amongst 17 rings centered on the beam axis (fig. 1). The first ring (2°-3°) which may sustain a high flux of elastically scattered particles is made of 12 fast counting phoswich scintillators (0.5 mm thick NE102 plastic followed by a 25 cm long NE115 plastic). From 3° to 45°, due to the required large energy dynamics , rings 2 to 9 comprise 180 three stage telescopes each made of an axial field 5 cm deep ionization chamber operated at 50 mb

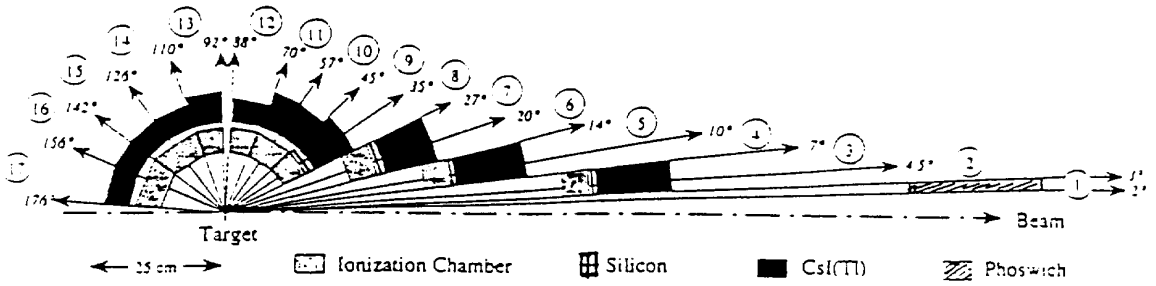

Figure 1: Schematic view of the INDRA detector showing the different elements arranged in a ring structure. The beam axis is an axis of symmetry for the detector.

of C_3F_8 gas, a 300 μm thick silicon detector and an ICs crystal deep enough to stop all particles. The angular range from 45° to 176° is covered by rings 10 to 17 made of 144 two-stage telescopes each consisting of an axial field ionization chamber operated at 30 mb and an ICs crystal scintillator. All detector signals are treated through specifically designed and highly integrated modules, most of which are in the VXIbus standard. This allows full remote control of the detector parameters, including visualization of signals. Constant monitoring of the detector stability is ensured using a pulsed laser source and electronic pulsers. Great care has been given to the energy calibration of all detection modules, making use of specific detectors and of the secondary beams delivered by the GANIL accelerator. For fragments with $Z>3$, charge identification is made through the usual ΔE-E method up to $Z\approx50$, down to an energy threshold of ~1 AMeV for $Z<10$ and ~1.7 AMeV for $Z>10$. For elements with $Z\leq3$, isotopic separation is achieved in the ICs crystals using pulse shape discrimination techniques.

Beams of ^{36}Ar produced by the GANIL facility were used to bombard a 193 μg/cm^2 thick self-supporting ^{58}Ni target. In order to maintain the probability for multiple interactions in the target below 10^{-4}, the beam intensity was maintained around $3\text{-}4\times10^7$ pps. Data were taken using a minimum bias trigger based on the multiplicity M such that events where registered for $M\geq3$ for bombarding energies up to 74 AMeV and $M\geq4$ above. For normalization purpose data were also acquired without any bias ($M\geq1$) at 52 AMeV bombarding energy.

In figs. 2a-b), the total detected charge, Z_{tot}, is presented as a function of the total measured momentum, P_z, along the beam direction relative to the beam momentum, P_0, at 32 and 95 AMeV incident energies. Three regions are visible on these diagrams. For $Z_{tot}<18$ and $P_z/P_0<0.5$, neither the quasi-projectile nor the quasi-target have been detected. This corresponds to the most peripheral collisions in which the projectile is scattered at angles smaller than 2^0 and the recoiling target does not have enough energy to overcome the detector thresholds. For $18<Z_{tot}<28$ and $P_z>0.5$, the quasi-projectile is detected but the quasi-target is still too low in energy. Finally, for $Z_{tot}>28$, and $P_z/P_0> 0.6$, both the quasi-projectile and the quasi-target are observed. In this latter region the missing charge can be inputted for one part to the detector efficiency (geometrical

cover and detection thresholds) and for another part, to the multi-hit probability which increases with the multiplicity. Besides the above mentioned effects, obviously, non detected neutrons

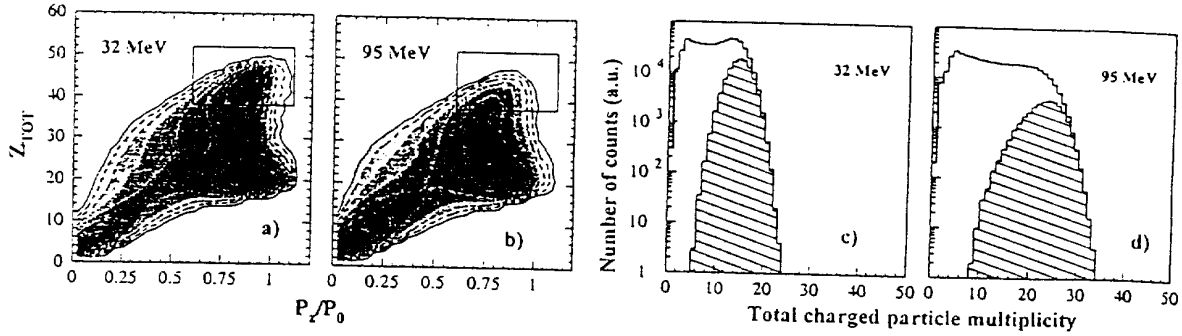

Figure 2 : a-b) Total detected charge versus the fraction of the beam momentum detected along the beam axis at (a) 32 and (b) 95 AMeV bombarding energies. Selected quasi-complete events are indicated by the rectangles. **c-d)** Measured total charged particle multiplicity distributions (full curves) and the multiplicity distributions for quasi-complete events (hatched histograms).

contribute also to the missing momentum. The total charged particle multiplicity distributions measured at 32 and 95 AMeV are shown by the full curves in figs. 2c-d).

In the following, except when specified otherwise, we will consider only quasi-complete events in which more than 80% of the total charge (46) of the system and more than 60% of the incoming beam momentum have been detected, as indicated by the rectangles in figs. 2a-b). The corresponding multiplicity distributions are indicated by the hatched histograms in figs. 2c-d). These requirements eliminate mainly low multiplicity events corresponding to the most peripheral collisions.

As a measure of the violence of the collisions, we use the transverse kinetic energy ,E_{tr}, defined as:

$$E_{tr} = \sum_{i=1}^{i=M} K_i \sin^2 \theta_i \quad ,$$

where for a given event, the sum runs over all detected particles and where K_i and θ_i are respectively the kinetic energy and emission angle of particle *i*. The larger is E_{tr}, the more violent is the collision. In fact, as shown by simulations, the transverse energy is strongly correlated with the impact parameter. Assuming that the reaction cross-section $\sigma_R(b)$ up to an impact parameter b is essentially geometrical, $\sigma_R(b) = \pi b^2$, an estimate of the impact parameter can be obtained from the transverse energy through the relation:

$$\frac{b}{b_{\max}} = \left[\frac{1}{Y_{tot}} \int_{E_{tr}}^{E_{max}} \frac{dY}{dE_{tr}} dE_{tr} \right]^{1/2} ,$$

where $b_{max} \sim 9.6$ fm is the grazing impact parameter, Y_{tot} is the total measured yield whereas the integral represents the yield between the transverse energy E_{tr} and the maximum transverse energy E_{max}.

In fig. 3) are presented the charge distributions of the fragments with $Z \geq 3$ as a function of their parallel velocity along the beam direction at 32 and 95 AMeV bombarding energies for four

impact parameter bins. At all bombarding energies, from 32 AMeV to 95 AMeV, for most collisions (b>2.5fm, figs. 3a-b), the fragments are essentially located at velocities near the projectile or target velocities, emphasizing the binary character of these collisions. For the most

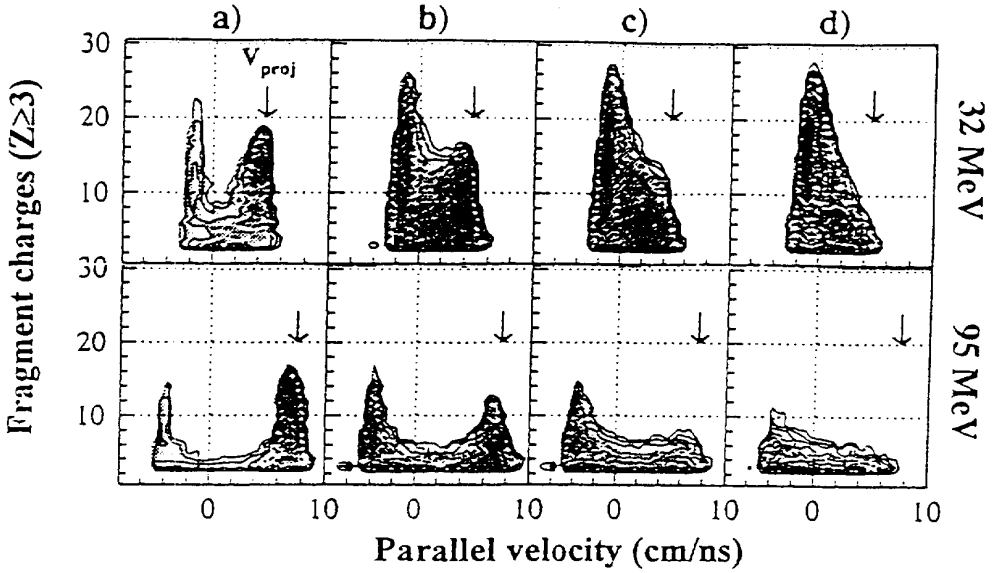

Figure 3 : Charge distributions of the fragments with Z≥3 as a function of their parallel velocity in the center of mass frame at 32 and 95 AMeV bombarding energies, for four impact parameters bins: a) 6.5 fm<b<4.5 fm, b) 4.5 fm<b<2.5 fm, c) 2.5 fm<b<1 fm, d) b<1 fm. The arrows indicate the projectile velocity.

central collisions (b<2.5fm, figs. 3c-d), at 32 AMeV incident energy, some heavy fragments are produced with a velocity close to the center of mass velocity, suggesting an incomplete fusion process which completely disappears above 52 AMeV. However, at all impact parameters, the presence of fragments at mid-velocity indicates some deviations from a purely binary process with an emission from the overlapping zone between projectile and target.

In order to determine the properties of the primary sources of emission, those have to be reconstructed from the kinematical properties of the detected fragments and particles. This was done, event by event, using the « Minimum Spanning Tree » (MST) technique[9], which consists in finding the minimum path linking N points in a metric space. For the present analysis[10], the method was applied in the velocity space where the « distance » between two particles is defined as the square of their relative velocity:

$$d_{ij} = V_{ij}^2 = \frac{(\vec{\beta_i} - \vec{\beta_j})^2 - (\vec{\beta_i} \times \vec{\beta_j})^2}{(1 - \vec{\beta_i}\vec{\beta_j})^2} \quad ,$$

where $\vec{\beta_i}, \vec{\beta_j}$ are the velocities of particles i and j respectively. As the origin of Z=1 particles is not well defined, the minimum tree is built using Z≥2 particles only. Then, the largest link which maximizes the thrust T_2 is broken to form two clusters. If no link gives T_2<0.65, it is assumed that the separation in two clusters is unreliable. The thrust[11], T_2, is defined in the center of mass frame as follows:

$$T_2 = \frac{\left|\sum_{i \in S_1} \vec{p}_i\right| + \left|\sum_{j \in S_2} \vec{p}_j\right|}{\sum_{k \in S_1 \cup S_2} \left|\vec{p}_k\right|} \quad ,$$

where $\vec{p}_i, \vec{p}_j$ are the momentum of particles i and j attributed to sources 1 or 2 respectively.

Once this procedure is achieved, the hydrogen isotopes are distributed amongst the two clusters on proximity criteria. The properties of the emission sources thus obtained were tested against different reconstruction techniques[12,13] which were found to yield essentially the same results. Taking into account the detection efficiency, the average charges and masses of the reconstructed quasi-projectile (QP) and quasi-target (QT) are very close to those of the initial projectile and target. However the width of the distributions increases from ~10% to ~20% by going from peripheral to central collisions. It is now possible to study the properties of each source.

3. Decay modes and energy sharing.

The amount of excitation energy, E^*, imparted to the QP or to the QT is determined event by event by calorimetry through the relation:

$$E^* = \sum_{i=1}^{M_c} K_i + \sum_{j=1}^{M_n} K_j - Q \quad ,$$

where M_C and M_n are the multiplicities of charged particles and of neutrons respectively. The value of M_n, which is not measured is deduced from mass and isospin conservation. K_i are the kinetic energies of each particle (in the source reference frame). The average kinetic energy K_n of the neutrons is taken as the average kinetic energy of the protons in the event minus 2 MeV to take into account the absence of Coulomb barrier. Finally, Q is just the mass balance.

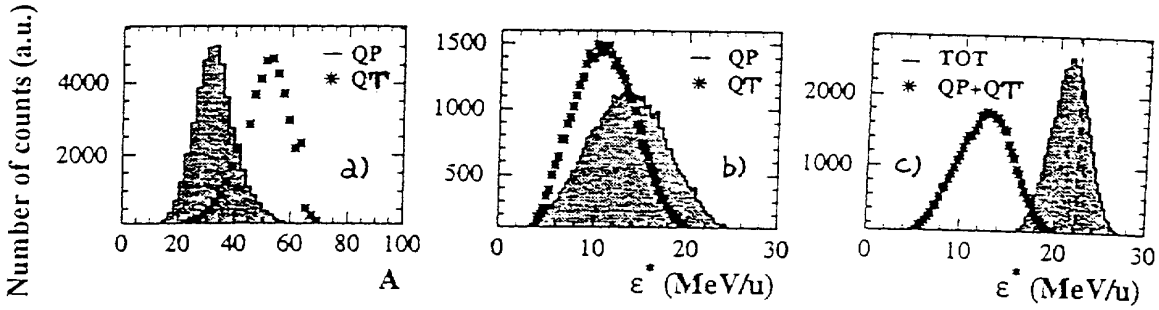

Figure 4 : Properties of the QP and QT deduced from quasi-complete events in the $^{36}Ar+^{58}Ni$ reaction at 95 AMeV bombarding energy. **a)** Mass distributions of the QP and of the QT. **b)** Excitation energy (per nucleon) distributions in the QP and the QT. **c)** Total excitation energy (per nucleon) distribution in the system (QP+QT) and total reconstructed energy (excitation energy + relative energy). The c.m. available energy is indicated by the vertical dashed line.

Some features of the QP and QT, for quasi-complete events in the $^{36}Ar+^{58}Ni$ reaction at 95 AMeV bombarding energy are shown in fig. 4). The QP and QT mass distributions (fig. 4a), not corrected for detector efficiency, are relatively broad but remain peaked close to the masses of the

projectile and target respectively. The QP and QT excitation energies (fig. 4b) cover a broad range, extending from ~4 AMeV to ~25 AMeV and from ~4 AMeV to ~20 AMeV respectively. From these spectra, it has to be noted that the QP carries an amount of excitation energy per nucleon somewhat larger than the QT. In fig. 4c), the total excitation energy imparted to the QP and QT is compared to the total energy, E_{tot}, reconstructed in the center of mass of the system. For a perfect detection system, E_{tot} should be equal to the c.m. available energy (22.3 AMeV). The width of the E_{tot} spectrum can be considered as a measure of the overall precision of the method. The difference between the total energy, E_{tot} and the total excitation energy imparted to QP and QT is just the energy of relative motion between QP and QT.

Figure 5) depicts the decay modes of the QP, the QT and the whole system as a function of the excitation energy per nucleon, ε^*. Here, a fragment is defined as a nucleus with $Z \geq 3$. For each excitation energy bin, are reported the probabilities $P_n(\varepsilon^*)$ of n-fragment emission, with $0 \leq n \leq N$ where N is the maximum number of observed fragments. For a given ε^* the $P_n(\varepsilon^*)$ add to one. At low excitation energies the QP and the QT decay mainly by light particle emission leaving only one heavy residue. The partition in two heavy fragments (fission-like process) is about two times more probable for the QT than for the QP. These two partitions evolve slowly with excitation energy.

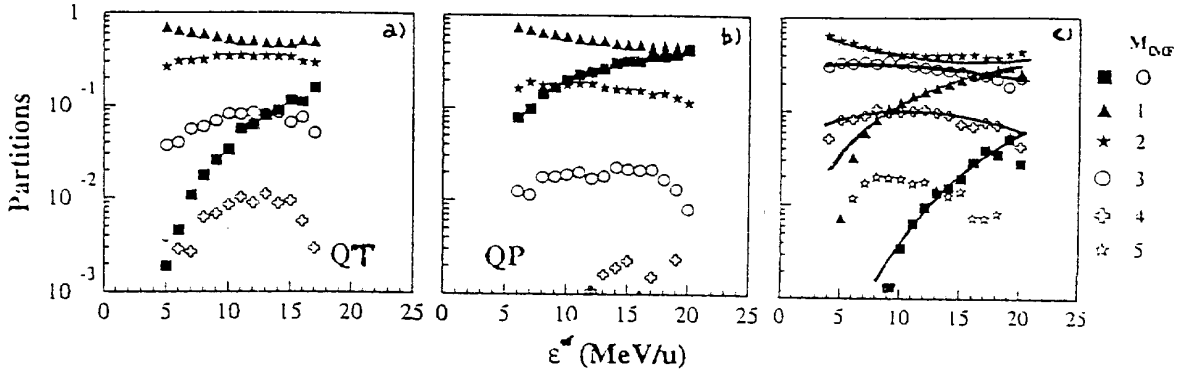

Figure 5 : Decay modes of the QP (a), the QT(b) and the whole system (c) as a function of the excitation energy in the reaction $^{36}Ar+^{58}Ni$ at 95 AMeV incident energy.

Higher-order partitions increase rapidly with excitation energy to reach a maximum at $\varepsilon^* \sim 10$ AMeV and then decrease. The most dramatic evolution is seen in the no-fragment partition which increases continuously with excitation energy to become the dominant decay mode of the QP at the highest excitation energies. This particular mode corresponds to a complete disintegration into light particles. The partitions of the whole system (QP+QT) as a function of the excitation energy ε^* are shown in fig. 5c). Obviously, the two-fragment partition is now predominant emphasizing the binary character of the reaction. For a given excitation energy ε^* in the total system, these partitions can be deduced from the partitions of the QP and of the QT at the corresponding excitation energies ε^*_{QP} and ε^*_{QT}, using the relation:

$$P_n^{tot}(\varepsilon^*) = \sum_{i=0}^{n} P_i^{QP}(\varepsilon^*_{QP}) P_{n-i}^{QT}(\varepsilon^*_{QT}) \quad ,$$

where, P_n^{tot} , P_i^{QP} and P_{n-i}^{QT} are respectively the probabilities for partitioning the whole system into n fragments, the QP into i fragments and the target into n-i fragments. The partitions thus calculated for $0 \leq n \leq 4$, are indicated by the full curves in fig. 5c). The agreement with the data is excellent, indicating that the QP and the QT decay independently from one another.

In fig. 6) the excitation energy, ε^*_{QT} in the QT is plotted versus the excitation energy, ε^*_{QP} in the QP, as a function of the violence of the collisions given by the transverse energy, E_{tr}, for the reactions ^{36}Ar+KCl and ^{36}Ar+^{58}Ni at 52 and 74 AMeV bombarding energies. For a symmetric system such as Ar+KCl, whatever the excitation process one expects $\varepsilon^*_{QP} = \varepsilon^*_{QT}$. This is indeed the case, showing that neither the detector nor our analysis method introduce any bias. This important point was also checked through intensive simulations. For the Ar+Ni reaction on the contrary, the temperature of the QP is higher than the temperature of the QT ($\varepsilon^*_{QP} > \varepsilon^*_{QT}$). This suggests that the thermalization time is greater than the interaction time, $\tau_{int} < 100$ fm/c. For the sake of comparison, taking into account the evolution of the masses of the QP and of the QT respectively with impact parameter, equal sharing of the total excitation energy ($E^*_{QP}=E^*_{QT}$) is indicated by the dashed lines in fig. 6). Then, the question arises to which extent the QP and the QT reach thermodynamical equilibrium before decaying. We will try to give some answer to this question in the following.

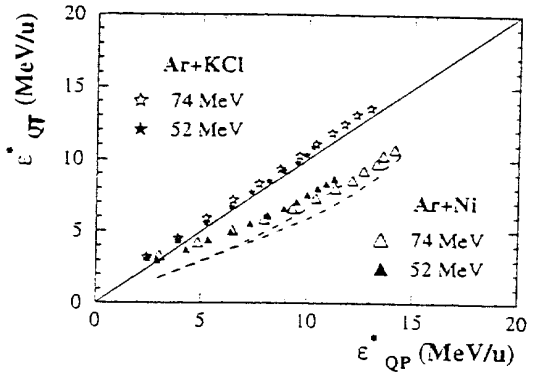

Figure 6 : Sharing of the excitation energy between the QP and QT as a function of the violence of the collision.

4. Vaporization events.

Vaporization events in the reaction ^{36}Ar+^{58}Ni, are defined as events in which only light particles ($Z \leq 2$) are produced. In order to ensure that the probability that a heavy fragment may have escaped detection is below 10%, only events with a total detected charge greater than 41 were kept. Such events have been extensively studied by the collaboration[12,14,15] and we will recall here only the main results. Vaporization of the whole system set-in at ~ 50 AMeV bombarding energy to reach[14] about 2×10^{-3} of the reaction cross-section at 95 AMeV. It as been shown[12] that at least 90% of these events result from the separate vaporization of the QP and of the QT. After source reconstruction, in agreement with the results presented fig. 6) on energy sharing, it is found that the QP is hotter than the QT. By increasing the bombarding energy from 52 to 95 AMeV, the average excitation energy $\langle\varepsilon^*_{QP}\rangle$ imparted to the QP, increases from 10.1 AMeV to 17.7 AMeV whereas for the QT, $\langle\varepsilon^*_{QT}\rangle$ increases from 8.8 AMeV to 14.6 AMeV. Once again, the question arises whether or not thermodynamical equilibrium is reached before the QP and the QT decay.

To answer this question, the properties of the decay products of the QP have been investigated in detail[15].

In the QP c.m. frame, for each particle species, the forward and backward kinetic energy spectra are superimposable. All these spectra present exponential tails, the slopes of which do not differ by more than 30% from one particle type to an other. The average kinetic energies of these particles increase almost linearly with excitation energy and are equal within 20%. Very similar results are obtained for the QT. For the emission from a thermalized source one expects not only a forward-backward symmetry but also, except for Coulomb effects, the same average kinetic energy for all particles. The observed deviations may have several origins such as recoil effects and side-feeding which should be assessed.

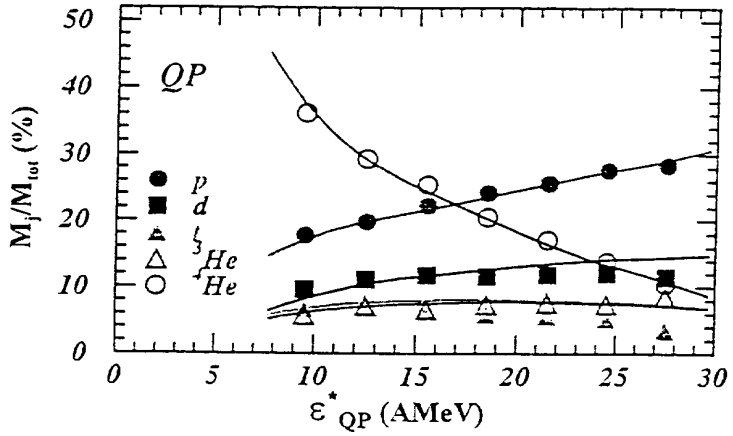

Figure 7 : Contribution of the different particle species to the decay of the vaporizing QP as a function of its excitation energy. The curves are the result of the model calculation (see text).

The composition of the decay products of the QP is shown in fig. 7) where the ratio M_i/M_{tot} between the multiplicity M_i of species i and the total multiplicitty M_{tot} (including neutrons) is plotted as a function of the excitation energy ε^*_{QP}. The abundance of α-particles which dominate at low excitation energy decreases rapidly with excitation energy and is mainly compensated by an increase of the proton yield. The deuteron relative abundance stays roughly constant. Whereas the ^{3}He yield increases slightly, the tritons follow the opposite trend. This data are compared to the prediction of the CEM model of ref.[16] in which the emitting source is viewed as a nuclear gas of particles (fermions and bosons) in thermal as well as in chemical equilibrium at density ρ and temperature T. The population densities of the different nuclear species are completely determined from the conservation laws and the equilibrium distribution in the macrocanonical ensemble :

$$n_i = \frac{g_i (m_i T)^{3/2}}{\sqrt{2}\pi^2\hbar^3} \times \int_0^\infty dz \sqrt{z} (\exp(z - \frac{\mu_i}{T_{ini}} + \frac{E_i}{T_{ini}}) \pm 1)^{-1} \quad ,$$

where m_i, g_i, E_i and μ_i are respectively the mass, the degeneracy factor, the intrinsic energy (ground state plus excitation energy) and the chemical potential of particle species i which is a function of the break-up density ρ via the neutron and proton chemical potentials μ_n and μ_p. The signs + or − apply to Fermi or Bose statistics respectively. T_{ini} is the initial temperature. Corrections to an ideal gas are also included in the form of an excluded volume. The freeze-out

density has been fixed to $\rho=\rho_0/3$ in order to reproduce the proton to alpha yield ratio. All nuclei up to ^{20}Ne and their known excited states with a width $\Gamma \leq 2$ MeV were introduced in the calculation and the final distributions corrected for resonance decay. The results of this calculation in excellent agreement with the data are shown by the full curves in fig. 7). The experimental excitation energy range was covered by varying the temperature from 10 to 25 MeV. The calculated average kinetic energies of the different particles are also rather well reproduced[15]. All these facts strongly suggest that the QP and the QT have reached thermodynamical equilibrium before decaying.

5- The caloric curve of the quasi-projectile.

In order to be able to study the QP over a broad excitation energy range it is necessary to take into consideration the peripheral collisions in which only the decay products of the QP are well detected. This was done by abandoning the condition on the total detected charge but keeping the condition on the total parallel momentum[13]. After QP reconstruction its excitation energy was determined by calorimetry as already described. Temperatures were calculated from the yields Y of several pairs of light isotopes differing by one neutron, following the prescription of Albergo et al.[17] :

$$T_r = \frac{B}{\ln\left[a\dfrac{Y(Z,N)Y(Z+1,N)}{Y(Z,N+1)Y(Z+1,N)}\right]} \quad \text{and} \quad B = [B(Z,N)-B(Z+1,N)] - [B(Z,N+1) - B(Z+1,N+1)],$$

where Z and N are respectively the number of protons and neutrons for a given isotope whereas, $B(N,Z)$ is its binding energy. The coefficient a is related to the spins of the populated states and has been calculated assuming population of the ground states only[13]. At high temperature, excited states may contain a large fraction of the yield. These states may decay either by γ or particle emission and thus the measured yields are not those at the emission time. Therefore the temperature T_r is only an apparent temperature. Apparent temperatures were also obtained from the slope of the kinetic energy spectra. These apparent temperatures as well as those deduced from the yields of different isotope pairs are show in fig. 8) as a function of the QP excitation energy ε^*_{QP}. All these temperatures are different emphasizing the fact that they are only effective and are not a measurement of the initial temperature. In order to assess the origin of the differences, calculations where made with the CEM model[16] described previously. The results of these calculations are given by the full curves in fig. 8). Above $\sim\varepsilon^*_{QP}$=12 AMeV they are in fair agreement with the data, reproducing the observed trends. As expected, this multifragmentation model fails completely at low excitation energy where classical evaporation is expected[13]. In the calculation, the initial temperature T_{ini} was varied from 2 to 18 MeV. and follows the apparent temperature given by the slope of the deuteron spectra. From the calculation, it is found that the

differences between the different apparent temperatures originate from side-feeding and resonance decay. The inclusion of all excited states with a width $\Gamma \leq 2$ MeV was found essential to reproduce

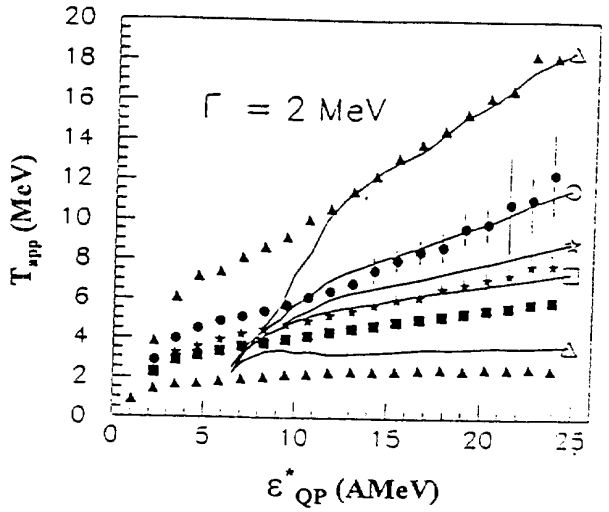

Figure 8 : Measured apparent temperatures versus excitation energy in the QP. The temperatures deduced from the slopes of the deuteron kinetic energy spectra are indicated by the upper triangles. All other temperatures have been obtained from various isotope pairs : ^{6}Li,^{7}Li-^{3}He,α (●), d,t-^{3}He,α (★) ; p,d-^{3}He,α (■) ; p,d-^{6}Li,^{7}Li(▲). The curves are the result of a model calculation as described in the text.

the data. Finally, none of the apparent temperature versus excitation energy curves show evidence for a plateau followed by a rise (first order liquid-gas phase transition) at high excitation energy as it as been reported in a recent experiment[18].

6- Summary.

The reaction ^{36}Ar+^{58}Ni has been studied in detail from 32 to 95 AMeV bombarding energy. Over this whole energy range, the reaction remains essentially binary in nature even for the most central collisions except below 50 AMeV where some fusion still occurs. Although the interaction time is too small to permit thermal equilibrium between the quasi-projectile and the quasi-target, these however are able to reach independently thermodynamical equilibrium before disintegrating. The decay modes of the quasi-projectile and quasi-target have been explored over a broad excitation energy range (up to 25AMeV). Multifragmentation seems to set in at ~ 12 AMeV excitation energy whereas vaporization of the total system begins to occur at ~ 6 AMeV. No evidence for a plateau as an indication of a liquid-gas phase transition was found in the caloric curve of the quasi-projectile.

References

1) S. Levit and P. Bonche Nucl., Phys. **A437** (1985) 426.

2) J. Besprosvany and S. Levit, Phys. Lett. **B217** (1989) 1.

3) L.G. Moretto and G.J. Wozniak, Ann. Rev. of Nucl. Part. Sci. 43 (1993) 379, and references therein.

4) J.P. Bondorf et al. Phys. Reports 257 (1995), and references therein.

5) *Nuclear Matter and Heavy-Ion Collisions,* Proceedings of the 1989 Les Houches Winter School, M. Soyeur, B. Tamain and M. Porneuf, eds. (Plenum; New York, 1989).

6) J. Pouthas et al., Nucl. Inst. and Meth. **A357** (1995) 418.

7) J.C. Steckmeyer et al., Nucl. Inst. and Meth. **A361** (1995) 472.

8) J. Pouthas et al., Nucl. Inst. and Meth. **A369** (1995) 222.

9) J.C. Gower and G.J.S. Ross, Appl. Statistics, **18** (1969) 54.

10) L. Nalpas, Ph.D thesis, Université de Paris XI, France, 1996.

11) J. Cugnon and D. L'Hote, Nucl. Phys. **A397** (1983) 519.

12) M.F. Rivet et al. Phys. Lett. **B388** (1996) 219.

13) Ma Y.-G. et al., Phys. Lett. **B390** (1997) 41.

14) Ch.O. Bacri et al., Phys. Lett. **B353** (1995) 27.

15) B. Borderie et al., Phys. Lett. **B388** (1996) 224.

16 F. Gulminelli and D. Durand, LPCC report 96-11 and Nucl. Phys. A., *in press.*

17 S. Albergo et al., Nuovo Cimento **A89** (1985) 1.

18 J. Pochodzalla et al., Phys. Rev. Lett. **75** (1995) 1040.